Peer-reviewed version available at Catalysts 2018, 8, 260; doi:10.3390/catal8070260

Article

Influence of the structure forming agent on the performance of Fe-N-C catalysts

Sven Schardt [1], Natascha Weidler [2], W. David Z. Wallace [1], Ioanna Martinaiou [2,3], Robert W. Stark [4] and Ulrike I. Kramm [1,2,3,*]

[1] TU Darmstadt, Department of Chemistry, Catalysts and Electrocatalysts group (EKAT), 64287 Darmstadt
[2] TU Darmstadt, Department of Materials and Earth Sciences, EKAT group, 64287 Darmstadt
[3] Graduate School of Excellence Energy Science and Engineering, 64287 Darmstadt
[4] TU Darmstadt, Department of Materials and Earth Sciences, Physics of Surfaces group, 64287 Darmstadt
* Correspondence: kramm@ese.tu-darmstadt.de; Tel.: +49-6151-1620356

Abstract: In this work the influence of the structure forming agent on the composition, morphology and oxygen reduction reaction (ORR) activity of Fe-N-C catalysts was investigated. As structure forming agent (SFA), dicyandiamide (DCDA) (nitrogen source) or oxalic acid (oxygen source) or mixtures thereof were used. For characterization, cyclic voltammetry and rotating disc electrode (RDE) experiments were performed in 0.1 M H_2SO_4. In addition to this, N_2 sorption measurements and Raman spectroscopy were performed for the structural characterization. The role of metal, nitrogen and carbon sources within the synthesis of Fe-N-C catalysts has been pointed out before. Here, we show that the optimum in terms of ORR activity is achieved if both N- and O-containing SFAs are used in almost similar fractions. All catalysts display a redox couple, whereat its position depends on the fractions of SFAs. The SFA has also a strong impact on the morphology: Catalysts that were prepared with a larger fraction of N-containing SFA revealed a higher order in graphitization, indicated by bands in the 2nd order range of the Raman spectra. Nevertheless, the optimum in terms of ORR activity is obtained for the catalyst with highest D/G band ratio. Therefore, the results indicate that the presence of an additional oxygen-containing SFA is beneficial within the preparation.

Keywords: Fe-N-C catalyst; oxygen reduction reaction

1. Introduction

Me-N-C catalysts play an emerging role as possible catalyst materials for the oxygen reduction reaction in fuel cells. It is clear, that they can be prepared from any kind of metal, nitrogen and carbon precursor, but that the overall achievable activity will be strongly related to the optimization of the mixtures. In the first approaches, macrocycles were supported on a carbon black and then pyrolysed at temperatures above 600 °C to form significantly more active catalysts in comparison to the non-pyrolysed macrocycles [1-2]. To enable cheaper preparation and independent optimization of metal and nitrogen content in the synthesis, alternative preparation approaches had to be established. In 1989, Gupta et al. showed that the combination of metal acetate with polyacrylonitrile and carbon black leads to the formation of active materials when pyrolysed at temperatures > 600 °C [3]. Main efforts to find suitable nitrogen and metal precursors were made by Dodelet's group and others [4-7]. These early approaches were strongly limited in the density of active sites, as the carbon black always displays a relative mass in the final catalyst that is not contributing in terms of active sites [8-11].

To overcome this limitation, the first method that enabled the preparation of Me-N-C catalysts without additional carbon support, is the oxalate-supported pyrolysis of porphyrins developed at the Hahn-Meitner-Institute in Berlin (now Helmholtz-Zentrum Berlin) [12]. In this approach oxalate works as a structure forming agent (SFA) as the final catalyst resembles its morphology [13-15]. In addition to this, the use of sulfur strongly affected the morphology and performance of the catalysts

Peer-reviewed version available at *Catalysts* **2018**, *8*, 260; doi:10.3390/catal8070260

[16-17]. Sulfur usually enables a higher porosity and lower graphitization [16, 18], but more important it was found to prevent carbide formation that was assigned to active site destruction by works of us and of others [17, 19-20]. That indeed excess iron was at the origin of active site destruction was further confirmed through an alternative strategy to prevent active site destruction [21]. Namely, instead of following the state-of-the art preparation protocol (pyrolysis plus acid leaching), the pyrolysis was interrupted at 550 °C (a temperature below the temperature limit for iron carbide formation), excess iron was removed by an acid leaching. Afterwards the synthesis was continued up to the usual end temperature followed by an additional acid-leaching. Indeed, such catalysts prepared with intermediate acid leaching (IAL) reach the same activities as the original sulfur-added catalysts.

Motivated by these findings, we started to develop a new synthesis route in our group that uses dicyandiamide (DCDA) as structure forming agent in combination with a nitrogen and iron precursor. In recent studies we varied the amount of sulfur within this synthesis [22]. The trends in kinetic current density as a function of S/Me ratio were similar to trends observed previously for the combination of iron oxalate with CoTMPP [23], with a maximum in ORR activity at S/Fe = 0.8. However, in contrast to these earlier finding, our new catalysts still contained considerable fractions of iron carbide in the optimum of ORR activity. Only for the highest S/Me ratios iron carbide formation was inhibited but iron sulfide species were formed [22]. This showed us, that while sulfur-addition strongly affects the achievable ORR activity, sulfur itself helps not to prevent iron carbide formation in our selected system.

In order to get more insights on the missing parameter that is required for further optimization, we focused on a molar ratio of S/Fe = 0.8 in this work and stepwise exchanged the DCDA with oxalic acid as alternative structure forming agent with strong similarities to the metal oxalates used at the Helmholtz-Center in Berlin (or previously Hahn-Meitner-Institute). The results show that by tuning the composition of the SFAs the activity and morphology is changing considerably.

2. Results and Discussion

In the following chapter, the composition of the precursor is expressed as the relative oxalate content which is the molecular fraction of oxalic acid in the overall sum of structure forming agent (SFA = oxalic acid and DCDA). In Figure 1a and 1b the yield and the BET surface area; respectively, are given as a function of the relative oxalate content within the SFA.

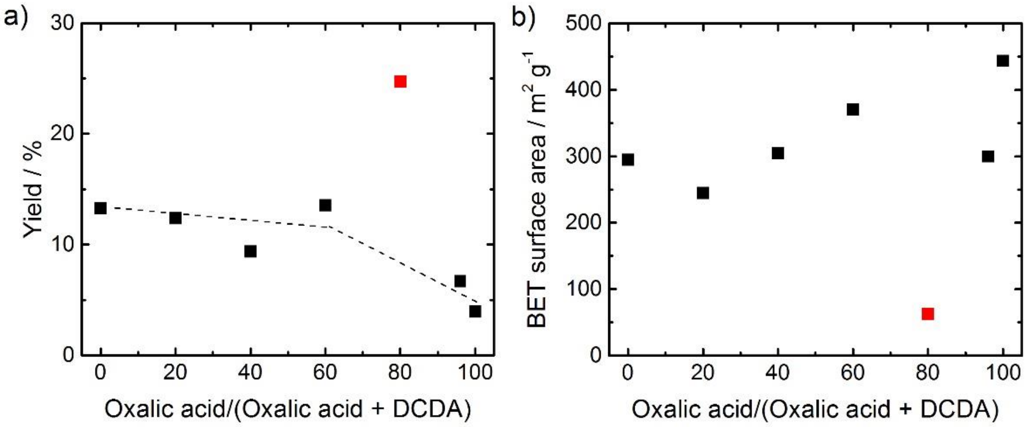

Figure 1. a) Change of the synthesis yield as a function of relative part of oxalic acid in the overall SFA (considering molar fractions) and b) relation between BET surface area and yield.

These values are obtained after pyrolysis and acid leaching. In general, the yields of final catalysts are larger when DCDA is used as SFA in comparison to oxalic acid. With respect to the BET surface area the trend looks almost inverse with higher surface area for the catalysts prepared with larger fractions of oxalic acid.

Peer-reviewed version available at *Catalysts* **2018**, *8*, 260; doi:10.3390/catal8070260

The data for the catalyst at 80 % oxalic acid as SFA is given in red color in both graphs. Initially, we assumed that these out-of-trend values of yield and BET surface area were due to failures during the synthesis of this catalyst. However, repeating the synthesis confirmed the reproducibility in terms of yield, BET and ORR activity. This catalyst (80 % oxalic acid in SFA) will not be included in the following discussion, as it seems that the precursor combination leads to undesired reactions, most probably already in the precursor stage. This is shortly addressed in section 3.1.

The results of N_2 sorption measurements are summarized in Table 1. As indicated, only some of the catalysts contain surface area within the micropore regime (< 20 nm), most of the samples are basically mesoporous.

Table 1. Summary of the results obtained from N_2 sorption measurements. SA is used as surface area.

Oxalic acid/ (Oxalic acid + DCDA)	100	96	80	60	40	20	0
BET SA / m² g⁻¹	444	300	63	371	305	245	295
Meso SA / m² g⁻¹	441	300	35	147	277	245	295
Micro SA / m² g⁻¹	3	< 1	28	224	28	0	0
Micro/BET / %	1	< 1	44	60	9	0	0

It becomes clear, that in order to obtain a significant fraction of micropores, both nitrogen and oxygen containing SFA should be used at the same time.

In order to see the impact of the synthesis on the electrochemical performance cyclic voltammetry and RDE experiments were performed in N_2 saturated; respectively O_2 saturated electrolyte. The results are given in Figure 2. It becomes clear that there is a strong impact of the SFA-ratio on the capacitive current density. Interestingly, all catalysts exhibit a redox peak at about 0.7 V. Furthermore, for some catalysts a peak in the anodic sweep is visible between 0.3 V and 0.4 V. This peak was also previously observed for phenanthroline-based catalysts but usually vanishes upon cycling. So far, we were not able to make a final assignment. For the intense redox peak at ~ 0.7 V it might be assigned either to Fe^{2+}/Fe^{3+} couple or quinone/hydroquine [11]. Considering the double layer capacity it roughly seems to increase with increasing ratio of oxalic acid (maximum for the sample with a ratio of 60 %) and then to drop down (see discussion of Figure 4a, below).

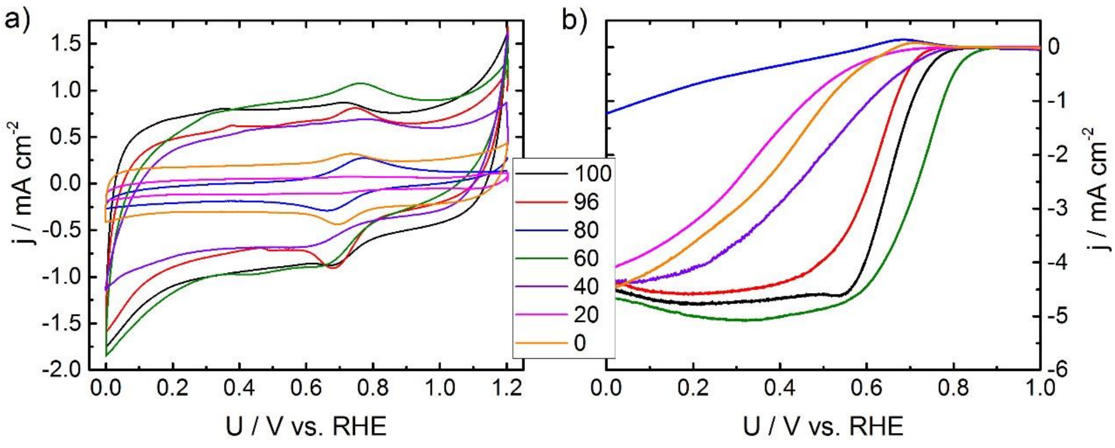

Figure 2. Cyclic voltammetry (100 mV s⁻¹) in N_2 saturated 0.1M H_2SO_4 (a) and rotating disc electrode experiments (rpm1500, 10 mV s⁻¹) (b) of the variation series.

During RDE experiments it is again the 60 % sample that gives the highest onset potential and largest kinetic current density in comparison to all other samples. Most of the samples give the usual shape of RDE curves, but at lower fractions of oxalic acid the curves indicate some kinetic hindrance.

Peer-reviewed version available at Catalysts 2018, 8, 260; doi:10.3390/catal8070260

Both, the CV and RDE curves of the outlier related to 80 % look pretty much like iron oxide species.

In Figure 3 the Tafel plots of all investigated catalysts are shown. It becomes apparent that the ORR activity in terms of kinetic current density changes drastically with the ratio of oxalic acid in the SFA. The Tafel slopes of the more-active catalysts give values of about 70 mV dec^{-1}. This value is in good agreement with the values that were observed for other catalysts prepared by the (oxalate supported) pyrolysis of porphyrins [15, 24-25] as well as alternatively prepared catalysts (without the use of a reactive gas heat-treatment) [19]. When the fraction of oxalic acid goes down the Tafel slope increases, getting closer to 100 mV dec^{-1}. While not intended, this might be related to an interaction of the catalyst with ammonia (from DCDA decomposition) during the heat-treatment. A larger Tafel slope value for catalysts that involve ammonia in their preparation was also previously observed [19].

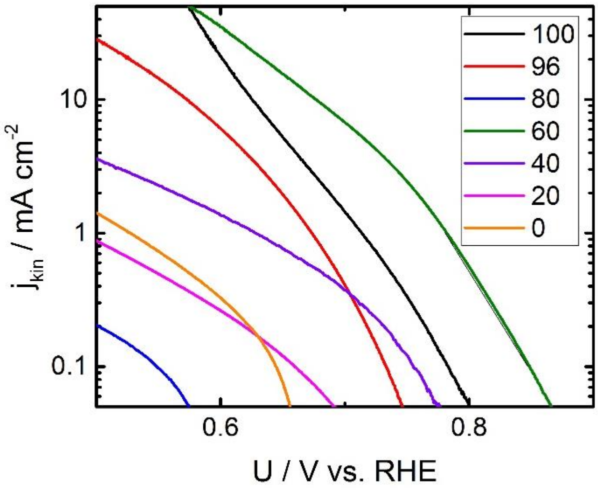

Figure 3. Tafel plots of all investigated catalysts (calculated from RDE data provided in Figure 2b).

As mentioned above, the capacity of the different catalysts seems to be affected by the ratio of oxalic acid in the SFA. A plot of the related current density in the double layer region of the CVs (named as j(DL capacity)) vs ratio of oxalic acid in SFA shows that there is a maximum in capacity current for 60 % oxalic acid in the SFA and then the capacitive current remains constant or slightly decreases, this is shown in Figure 4a. In contrast to this a clear maximum is visible for the ORR activity in Figure 4b.

In Figure 4c the potentials related to the peak maxima in the anodic sweep of the cyclic voltammograms are given as a function of the ratio of oxalic acid in the SFA. Roughly, the trend is similar as for the kinetic current density: The resulting kinetic current density is as higher as the the anodic peak position is, what is in agreement with previous reports [26-28]. Nevertheless, it becomes clear, that E(Peak$_{anode}$) is only a weak activity descriptor for this group of catalysts. While the peak position might be an indicator for the turn-over frequency (TOF) on active sites, the charge under the redox peak might be related to the number of active sites (if assigned to Fe^{2+}/Fe^{3+}) , or number of sites promoting the ORR (evtl. quinone/hydroquinone). As both (TOF and site density) will contribute to the kinetic current density, this might explain the only weak correlation. Furthermore, it should be noted, that the difference between the anodic and cathodic peak is not constant but increases from about 40 mV to 220 mV and then decreases to about 50 mV (not displayed). Further characterization will be required to fully understand this trend.

For characterization of the carbon morphology, Raman spectra were recorded for all catalysts (Figure 5a and b). The analysis of the Raman spectra was made in relation to literature on carbon blacks [29-30]. All samples reveal the typical shape of carbon blacks with distinct D-band and G-band intensities. While the latter is related to in-plane vibration modes, the former is related to vibrations “at the edges” of the graphene layer [31]. Hence, the intensity ratio D/G is inverse proportional to the graphene layer extension.

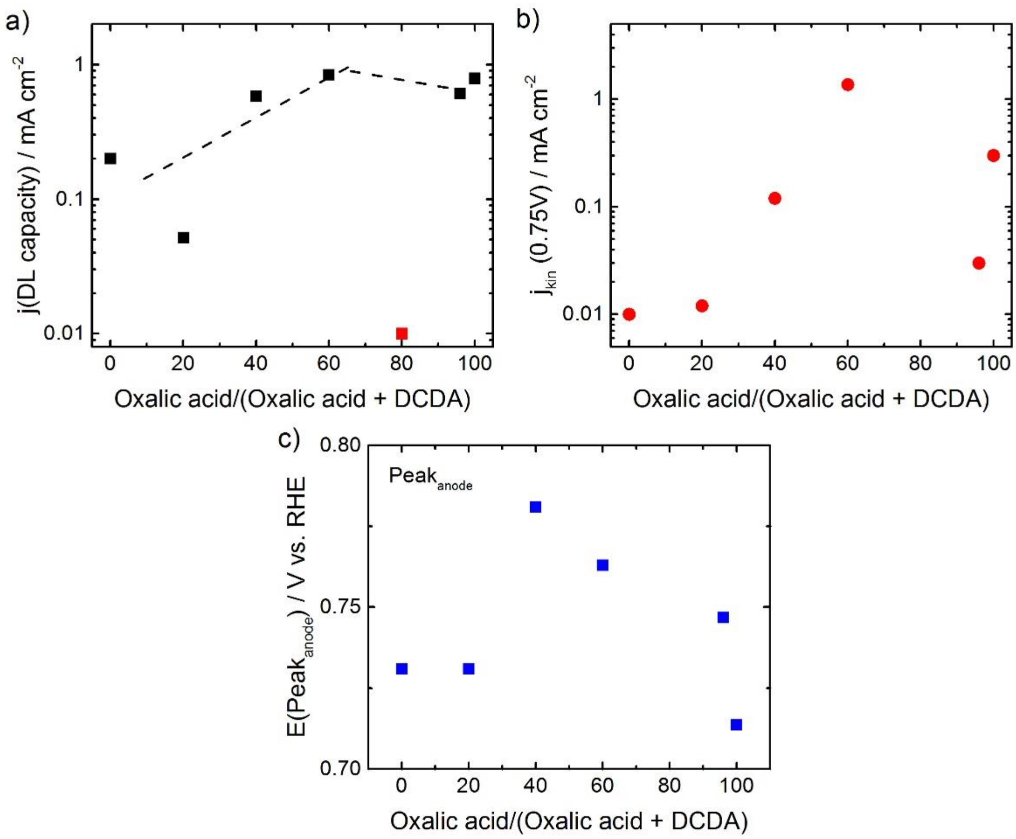

Figure 4. Analysis of electrochemical data. In (a) the current density related to the double layer capacity (100 mV s^{-1}), in (b) the kinetic current density j_{kin} and in (c) the potential positions of the peak maxima in the anodic sweep of the CVs are given as a function of the ratio of oxalic acid in SFA.

It is interesting to note, that for those samples with dominant ratios of DCDA in the SFA additional bands in the 2nd order region become pronounced. This band is related to the 2D band. In a recent work by Larouche et al. [32] it was discussed that the ratio of 2D/D areas can be used to calculate a graphene layer extension labelled L_{eq} that also considers the curvature within graphene flakes [32]. That is why in the paragraph above “at the edges” was written in quotation marks, because the D band will be formed when the vibrations occur at the edges, but also if the symmetry (e.g. by implementation of defects, 5-ring groups etc.) is broken.

Also the 1st order region was analyzed in more detail by fitting the spectra assuming the presence of four bands. The aforementioned D and G bands and in addition a D_3 and a D_4 band. These are assigned to heteroatoms in carbon and polyaromatic hydrocarbons, respectively [29-30, 32]. As an example, the fit of the most active catalyst is provided in Figure 5c.

In Figure 5d the intensity ratios of D/G band and D_3/G band are shown as a function of oxalic acid in the SFA. Except for the sample prepared exclusively with DCDA, first an increase in D/G ratio and then a decrease (above 60 % oxalic acid) is observed. Comparing the trends in Figure 4a and Figure 5d it seems that the intensity ratio D/G follows the trend in capacity. There is also a strong relation between the capacity and the BET surface area (not shown) underlining that in most of the cases indeed edges of graphene layers might contribute to the D-band intensity (rather than curvatures).

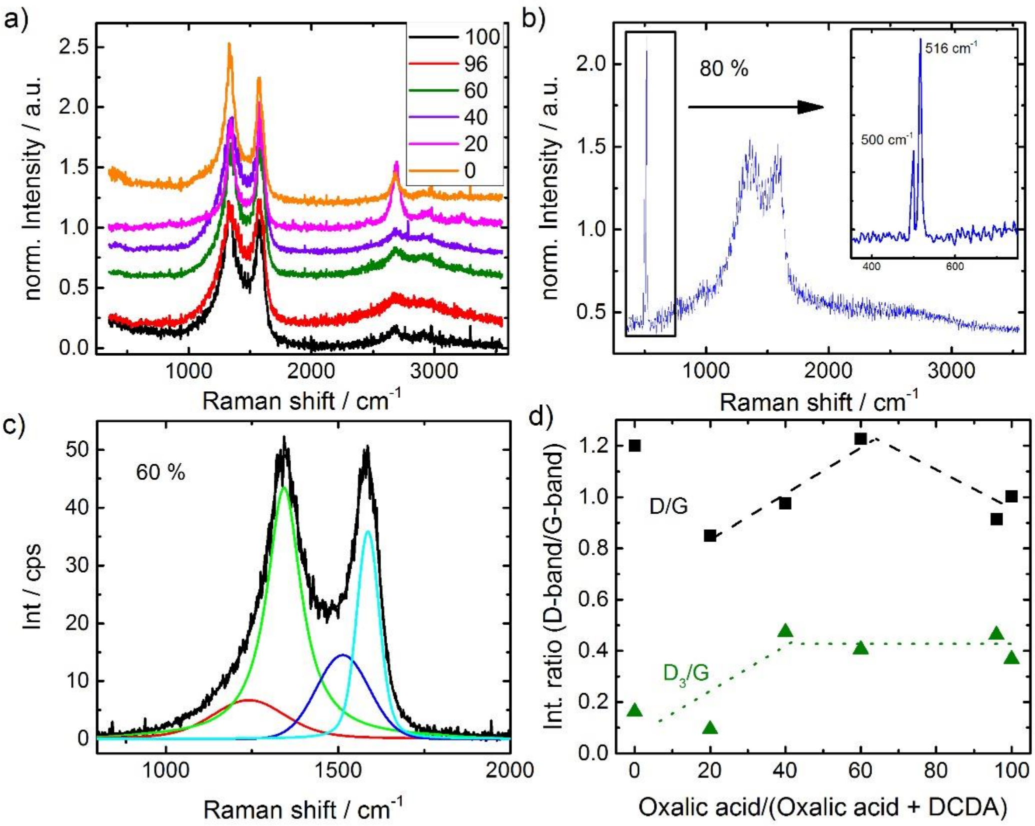

Figure 5. Raman spectra of the variation series (a), spectrum for 80% oxalic acid in SFAs (b) and deconvoluted Raman spectrum (1st order region) of the best performing catalyst with 60 % oxalic acid in SFAs (c). Influence of the ratio of oxalic acid in the SFA on the D/G and D_3/G band ratios (d).

In a previous work, we were able to show by analyzing the Raman spectra of a group of Me-N-C catalysts before and after accelerated stress tests (AST), that a decrease in the D_3/G ratio correlated with the decrease in ORR activity observed during AST [33]. As this loss in activity was also correlating with the out-of-plane displacement of metal out of the N_4 plane, we attributed a contribution of MeN_4 related vibrations to be located in the D_3 band region [33]. As given in Figure 5d, up to a ratio of 40 % oxalic acid in the SFA the D_3/G band ratio is increasing and then does not change significantly. On the basis of our previous work, this might be an indicator for a change of the relative amount of FeN_4 sites. The formation seems suppressed in case of ordered carbon rather than amorphous carbon that is found for the catalysts prepared with higher ratios of oxalic acid in the SFA.

Even though, it was already discussed above, that the sample with 80 % is out of trend, shortly its Raman spectrum as displayed in Figure 5b should be discussed. Distinct bands can be identified at 500 and 516 cm^{-1}. On first view, these bands were assigned to iron oxide vibrations [34]. This is in agreement with the band at 500 cm^{-1}, but so far we were not able to assign the band at 516 cm^{-1}. On the basis of the observations made so far for this sample, we believe that the formation of these two bands are in strong relation to its worse composition and activity.

Why does the activity increase so much by changing the fraction of oxalic acid in the SFA?

In our previous publication, the iron acetate was the only source of oxygen within the synthesis. In this study we replaced the iron acetate by iron chloride which allowed us to systematically vary the content of oxygen in the overall precursor from zero to a maximum of 70 at% (hydrogen not considered). It is interesting to note, that the catalyst with the maximum activity in this work has a relative content of oxygen (44 at%) very similar to the one calculated for the precursor of the oxalate support pyrolysis of porphyrins (43 at%). This might be an indicator for its very good performance.

Peer-reviewed version available at *Catalysts* **2018**, *8*, 260; doi:10.3390/catal8070260

Furthermore, the results indicate that only by using relative fractions of oxalic acid ≥ 40 % in the SFA, a sufficiently amorphous carbon is formed that enables high kinetic current densities.

3. Materials and Methods

3.1 Catalyst preparation

In order to prepare a precursor, first sulfur (0,78 mol eq) is grounded in a mortar together with iron chloride hexahydrate (1 mol eq). Then, 1,10-phenanthroline (0.48 mol eq) is added and mixed until a homogeneous mixture is obtained. Finally the structure forming agent (SFA) (6.5 mol eq) are added and the mixture is grounded until homogeneous. The preparation is given as Scheme in Figure 6, below.

As mentioned in the scheme, the color of the precursor changed upon addition of DCDA and/or oxalic acid. At the same time the initially solid precursor mixture turned into a viscose paste. While DCDA addition gave a distinct red color to this pulp (might be indicative of $[Fe(CN)_6]^{3+}$ formation), the addition of oxalic acid turned the color more orange/light brown. In addition, gas evolution took then place. If the precursor was then left in air, finally the precursor appeared like a meringue as visible in the picture. Regarding the precursor to obtain the 80 % catalyst of this variation series, it contains the minimum amount of DCDA that had to be present to enable this gas evolution. Gas evolution and formation of this meringue-like morphology was not observed at higher oxalic acid contents. Except for this; however, the precursor of the 80 % sample behaved rather similar during preparation compared to the other samples.

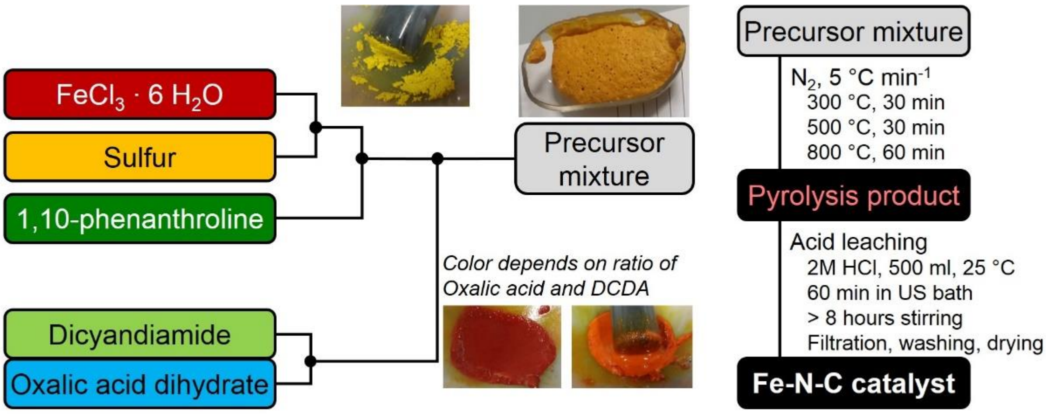

Figure 6. Scheme of the preparation procedure to obtain Fe-N-C catalysts by the use of two different type of SFA.

The as-obtained precursor mixture is filled in a quartz boat and then subjected to a heat-treatment. For the pyrolysis a heating ramp of 5 °C min^{-1} is chosen. To allow the system to balance in-between there are two dwell times at 300 °C and 500 °C, each for 30 min, before heated to the final end temperature of 800 °C with a dwell time of 60 min.

After cooling down (< 80 °C) the quartz boat with the pyrolysis product is transferred to 2M HCl. The composition is first acid-leached for 1 hour in an ultrasonic bath and then further stirred for additional 8 hours (usually over-night). After filtration, washing with H_2O and drying the final mass is obtained. Note, for determining the yield the final catalyst mass was divided by the precursor masses of iron chloride hexahydrate, 1,10-phenanthroline and sulfur, without considering the masses of DCDA and/or oxalic acid. This was applied, as otherwise, due to the different molar masses of DCDA and oxalic acid also the absolute mass of the precursor mixture would have changed.

3.2 Electrochemical measurements

Electrochemistry is performed in 0.1 M H_2SO_4 with a conventional 3-electrode setup. The working electrode is a glassy carbon disc (0.196 cm^2) coated with the catalyst ink. As counter and reference electrode; respectively, a glassy carbon rod and a Ag/AgCl were used. All given potentials refer to the reversible hydrogen electrode (RHE). In order to prepare the catalyst ink, 5 mg of catalyst powder were dispersed in a mixture of 25 µl Nafion (5 wt%), 83,3 µl H_2O and 142 µl ethanol, hence the Nafion to catalyst ratio is 0.25. After 30 min of sonication the ink is homogenized with an ultrasound homogenizer. Then 5 µl of the ink are dropped on the GC disc and left to dry (catalyst loading: 0.5 mg cm^{-2}).

First measurements are performed in N_2 saturated electrolyte with a conditioning of the electrode (20 scans with 300 mV s^{-1} 0.0 V to 1.2 V). Then a CV is measured with 100 mV s^{-1}, this CV is used for evaluating the capacitive current density of our catalysts. In addition, one Linear Scan Voltammogram (LSV) is measured from 1.2 V to 0.0 V for later background correction of the RDE data with 10 mV s^{-1}.

After saturating the electrolyte for 15 – 20 min with oxygen, three LSVs are recorded in the same potential range with 0, 900 and 1500 rpm as rotation speed. After background correction, the kinetic current density j_{kin} is determined by equation 1.

$$j_{kin}(U) = [j_{Diff,lim} \cdot j(U)] \cdot [j_{Diff,lim} - j(U)]^{-1} \tag{1}$$

In this equation, $j_{Diff,lim}$ is the as-measured diffusion limiting current density. For those catalysts that do not display a pronounced diffusion plateau the current density at 0.0 V was chosen as $j_{Diff,lim}$. The parameter j(U) is the as-measured current density.

3.3 Raman spectroscopy

Raman spectroscopy was performed with an "alpha300 R" confocal Raman microscope (WITEC) with a laser wavelength of 532.2 nm. Spectra were recorded in a range of 0 to 4000 cm^{-1} as overlay of 10 scans each with 10 seconds of integration time. For the measurements, catalyst ink was dropped on a silicon disc and dried. For each sample measurements are performed at two to three different locations and the average graphs are plotted in this work.

For the fitting of the 1st order range typically found for carbon blacks (800 – 2000 cm^{-1}) four bands were introduced with Voigt line shape.

3.4 N_2 sorption measurements

In order to determine the BET surface area and micropore surface area (from V-t plots) of all catalysts, N_2 sorption measurements were made with a Autosorb-3B (Quantachrome). Previous to the measurements, the samples (about 100 mg of the catalyst powders) were degassed at 200 °C over-night. Only for some of the catalysts a micropore surface area was obtained.

Author Contributions: Conceptualization and Methodology, U.I.K.; Preparation and formal analysis, S.S.; Structural characterization, W.D.Z.W., S.S., I.M., R.W.S., N.W. Writing-Original Draft Preparation, U.I.K., S.S., N.W.; Writing-Review & Editing, all authors; Supervision, N.W.; Project Administration, and Funding Acquisition, U.I.K.

Funding: This research was funded by the German ministry of education and research (BMBF) by grant number 03XP0092. In addition, I.M. and U.I.K. like to acknowledge further funding by the Graduate School of Excellence Energy Science and Engineering (GSC1070) funded by the German research foundation (DFG).

Acknowledgments: In this section you can acknowledge any support given which is not covered by the author contribution or funding sections. This may include administrative and technical support, or donations in kind (e.g., materials used for experiments).

Conflicts of Interest: The authors declare no conflict of interest.

References

1. Jahnke, H.; Schönborn, M.; Zimmermann, G., Organic Dyestuffs as Catalysts for Fuel Cells. *Topics Curr. Chem.* **1976,** *61*, 133–182.
2. Bagotzky, V. S.; Tarasevich, M. R.; Radyushkina, K. A.; A., L. O.; Andrusyova, S. I., Electrocatalysis of the Oxygen Reduction Process on Metal Chelates in Acid Electrolyte. *Journal of Power Sources* **1977,** *2*, 233–240.
3. Gupta, S. L.; Tryk, D.; Bae, I.; Aldred, W.; Yeager, E. B., Heat-treated Polyacrylonitride-Based Catalysts for Oxygen Electroreduction. *Journal of Applied Electrochemistry* **1989,** *19*, 19–27.
4. Lalande, G.; Côté, R.; Guay, D.; Dodelet, J.-P.; Weng, L. T.; Bertrand, P., Is Nitrogen Important in the Formulation of Fe-based Catalysts for Oxygen Reduction in Solid Polymer Fuel Cells? *Electrochimica Acta* **1997,** *42* (9), 1379–1388.
5. Côté, R.; Lalande, G.; Guay, D.; Dodelet, J.-P., Influence of Nitrogen-Containing Precursors on the Electrocatalytic Activtiy of Heat-Treated Fe(OH)2 on Carbon Black for O2 Reduction. *Journal of the Electrochemical Society* **1998,** *145* (7), 2411–2418.
6. Faubert, G.; Côté, R.; Dodelet, J.-P.; Lefèvre, M.; Bertrand, P., Oxygen reduction Catalysts for Polymer Electrolyte Fuel Cells from the Pyrolysis of FeII Acetate Adsorbed on 3,4,9,10-Perylenetetracarboxylic Dianhydride. *Electrochimica Acta* **1999,** *44*, 2589–2603.
7. He, P.; Lefèvre, M.; Faubert, G.; Dodelet, J.-P., Oxygen Reduction Catalysts for Polymer Electrolyte Fuel Cells from the Pyrolysis of Various Transition Metal Acetates Adsorbed on 3,4,9,10 Perylenetetracarboxylic Dianhydride. *Journal of new materials for electrochemical systems* **1999,** *2*, 243–251.
8. Herranz, J.; Lefèvre, M.; Larouche, N.; Stansfield, B.; Dodelet, J.-P., Step-by-Step Synthesis of Non-noble Metal Electrocatalysts for O2 Reduction under Proton Exchange Membrane Fuel Cell Conditions. *J. Phys. Chem. C* **2007,** *111* (51), 19033–19042.
9. Jaouen, F.; Dodelet, J.-P., Turn-over Frequency of O2 Electro-reduction for Fe/N/C and Co/N/C Catalysts in PEFCs. *Electrochimica Acta* **2007,** *52* (19), 5975–5984.
10. Herranz, J.; Lefevre, M.; Dodelet, J.-P., Metal-Precursor Adsorption Effects on Fe-based Catalysts for Oxygen Reduction in PEM Fuel Cells. *Journal of the Electrochemical Society* **2009,** *156* (5), B593-B601.
11. Jaouen, F.; Herranz, J.; Lefèvre, M.; Dodelet, J.-P.; Kramm, U. I.; Herrmann, I.; Bogdanoff, P.; Maruyama, J.; Nagaoka, T.; Garsuch, A.; Dahn, J. R.; Olson, T. S.; Pylypenko, S.; Atanassov, P.; Ustinov, E. A., A Cross-Laboratory Experimental Review of Non-Noble-Metal Catalysts for Oxygen Electro-Reduction. *Applied Materials and Interfaces* **2009,** *1*, 1623–1639.
12. Bogdanoff, P.; Herrmann, I.; Hilgendorff, M.; Dorbandt, I.; Fiechter, S.; Tributsch, H., Probing Structural Effects of Pyrolysed CoTMPP-based Electrocatalysts for Oxygen Reduction via New Preparation Strategies. *J. New. Mat. Electrochem. Systems* **2004,** *7*, 85–92.
13. Herrmann, I.; Bogdanoff, P.; Schmithals, G.; Fiechter, S., Influence of the Molecular and Mesoscopic Structure on the Electrocatalytic Activity of Pyrolysed CoTMPP in the Oxygen Reduction. *ECS Trans.* **2006,** *3* (1), 211–219.
14. Herrmann, I.; Kramm, U. I.; Fiechter, S.; Bogdanoff, P., Oxalate Supported Pyrolysis of CoTMPP as Electrocatalysts for the Oxygen Reduction Reaction. *Electrochimica Acta* **2009,** *54*, 4275–4287.
15. Koslowski, U. I.; Abs-Wurmbach, I.; Fiechter, S.; Bogdanoff, P., Nature of the Catalytic Centres of Porphyrin Based Electrocatalysts for the ORR – A Correlation of Kinetic Current Density with the Site Density of Fe-N4 Centres. *J. Phys. Chem. C* **2008,** *112* (39), 15356–15366.
16. Herrmann, I.; Kramm, U. I.; Radnik, J.; Bogdanoff, P.; Fiechter, S., Influence of Sulphur on the pyrolysis of CoTMPP as electrocatalyst for the oxygen reduction reaction. *J. Electrochem. Soc.* **2009,** *156* (10), B1283-B1292.
17. Kramm, U. I.; Herrmann-Geppert, I.; Fiechter, S.; Zehl, G.; Zizak, I.; Dorbandt, I.; Schmeißer, D.; Bogdanoff, P., Effect of Iron-Carbide Formation on the Number of Active Sites in Fe-N-C Catalysts for the Oxygen Reduction Reaction in Acidic Media. *J. Mater. Chem. A* **2014,** *2* (8), 2663–2670.
18. Kiciński, W.; Dembinska, B.; Norek, M.; Budner, B.; Polański, M.; Kulesza, P. J.; Dyjak, S., Heterogeneous iron-containing carbon gels as catalysts for oxygen electroreduction: Multifunctional role of sulfur in the formation of efficient systems. *Carbon* **2017,** *116*, 655–669.
19. Kramm, U. I.; Lefèvre, M.; Larouche, N.; Schmeisser, D.; Dodelet, J.-P., Correlations between Mass Activity and Physicochemical Properties of Fe/N/C Catalysts for the ORR in PEM Fuel Cell via 57Fe Mössbauer Spectroscopy and Other Techniques. *J. Am. Chem. Soc.* **2014,** *136* (3), 978–985.
20. Zhang, S.; Zhang, H.; Liu, Q.; Chen, S., Fe-N doped carbon nanotube/graphene composite: facile synthesis and superior electrocatalytic activity. *Journal of Materials Chemistry A* **2013,** *1* (10), 3302–3308.

21. Kramm, U. I.; Zana, A.; Vosch, T.; Fiechter, S.; Arenz, M.; Schmeißer, D., On the structural composition and stability of Fe–N–C catalysts prepared by an intermediate acid leaching. *Journal of Solid State Electrochemistry* **2016,** *20* (4), 969-981.
22. Janßen, A.; Martinaiou, I.; Wagner, S.; Weidler, N.; Shahraei, A.; Kramm, U. I., Influence of sulfur in the precursor mixture on the structural composition of Fe-N-C catalysts. *Hyperfine Interactions* **2018,** *239* (1), 7.
23. Herrmann, I., *Innovative Elektrokatalyse: Platinfreie Kathodenkatalysatoren für Brennstoffzellen*. VDM (Verlag Dr. Müller): Saarbrücken, 2008; p pages 248.
24. Kramm, U. I.; Abs-Wurmbach, I.; Herrmann-Geppert, I.; Radnik, J.; Fiechter, S.; Bogdanoff, P., Influence of the Electron-Density of FeN4-Centers towards the Catalytic Activity of Pyrolysed FeTMPPCl-Based ORR-Electrocatalysts. *J. Electrochem. Soc.* **2011,** *158* (1), B69-B78.
25. Meng, H.; Larouche, N.; Lefèvre, M.; Jaouen, F.; Stansfield, B.; Dodelet, J.-P., Iron porphyrin-based cathode catalysts for polymer electrolyte membrane fuel cells: Effect of NH3 and Ar mixtures as pyrolysis gases on catalytic activity and stability. *Electrochimica Acta* **2010,** *55* (22), 6450–6461.
26. Li, J.; Ghoshal, S.; Liang, W.; Sougrati, M.-T.; Jaouen, F.; Halevi, B.; McKinney, S.; McCool, G.; Ma, C.; Yuan, X.; Ma, Z.-F.; Mukerjee, S.; Jia, Q., Structural and mechanistic basis for the high activity of Fe-N-C catalysts toward oxygen reduction. *Energy & Environmental Science* **2016,** *9* (7), 2418-2432.
27. Zagal, J. H.; Páez, M.; Tanaka, A. A.; dos Santos, J., J.R.; Linkous, C. A., Electrocatalytic Activity of Metal Phthalocyanines for Oxygen Reduction. *J. Electroanal. Chem.* **1992,** *339*, 13–30.
28. Zagal, J. H.; Ponce, I.; Baez, D.; Venegas, R.; Pavez, J.; Paez, M.; Gulppi, M., A Possible Interpretation for the High Catalytic Activity of Heat-Treated Non-Precious Metal Nx/C Catalysts for O2 Reduction in Terms of Their Formal Potentials. *Electrochemical and Solid-State Letters* **2012,** *15* (6), B90-B92.
29. Sadezky, A.; Muckenhuber, H.; Grothe, H.; Niessner, R.; Pöschl, U., Raman microspectroscopy of soot and related carbonaceous materials: Spectral analysis and structural information. *Carbon* **2005,** *43* (8), 1731–1742.
30. Robertson, J., Diamond-like amorphous carbon. *Materials Science and Engineering R* **2002,** *37*, 129–281.
31. Tuinstra, F.; König, J. L., Raman Spectrum of Graphite. *Journal of Chemical Physics* **1970,** *53* (3), 1126–1130.
32. Larouche, N.; Stansfield, B. L., Classifying nanostructured carbons using graphitic indices derived from Raman spectra. *Carbon* **2010,** *48*, 620–629.
33. Martinaiou, I.; Shahraei, A.; Grimm, F.; Zhang, H.; Wittich, C.; Klemenz, S.; Dolique, S. J.; Kleebe, H.-J.; Stark, R. W.; Kramm, U. I., Effect of metal species on the stability of Me-N-C catalysts during accelerated stress tests mimicking the start-up and shut-down conditions. *Electrochimica Acta* **2017,** *243*, 183–196.
34. Jia, L.; Harbauer, K.; Bogdanoff, P.; Herrmann-Geppert, I.; Ramirez, A.; van de Krol, R.; Fiechter, S., [small alpha]-Fe2O3 films for photoelectrochemical water oxidation - insights of key performance parameters. *Journal of Materials Chemistry A* **2014,** *2* (47), 20196-20202.